Nature Environment and Pollution Technology
An International Quarterly Scientific Journal

p-ISSN: 0972-6268
(Print copies up to 2016)
e-ISSN: 2395-3454

Vol. 23 | No. 1 | pp. 255-263 | 2024

Original Research Paper

https://doi.org/10.46488/NEPT.2024.v23i01.021

Open Access Journal

The Suitability of Fe_3O_4/Graphene Oxide Nanocomposite for Adsorptive Removal of Methylene Blue and Congo Red

Viet Cao*†, Phuong Anh Cao, Duy Linh Han**, Minh Tuan Ngo***, Truong Xuan Vuong**** and Hung Nguyen Manh***

*Faculty of Natural Sciences, Hung Vuong University, Nguyen Tat Thanh Street, Viet Tri 35120, Phu Tho, Vietnam
**Joint Russia-Vietnam Tropical Science and Technology Research Center, 63 Nguyen Van Huyen, Hanoi 122100, Vietnam
***Department of Manufacturing Engineering, Faculty of Mechanical Engineering, Thai Nguyen University of Technology, Thai Nguyen 250000, Vietnam
****Faculty of Chemistry, TNU-University of Science, Thai Nguyen City 24000, Vietnam
†Corresponding author: Viet Cao; caoviet@hvu.edu.vn

Nat. Env. & Poll. Tech.
Website: www.neptjournal.com

Received: 22-06-2023
Revised: 15-07-2023
Accepted: 02-08-2023

Key Words:
Fe_3O_4/GO nanocomposite
Methylene blue
Congo red
Adsorption

ABSTRACT

In this study, Fe_3O_4/GO nanocomposite was synthesized by hydrothermal method and tested for its efficiency in removing methylene blue (MB) and congo red (CR) from water. The synthesized nanocomposite was characterized using Fourier-transform infrared spectroscopy (FTIR), X-ray diffraction (XRD), and scanning electron microscopy (SEM). The optimal values for MB and CR removal were determined to be pH 6.0, an adsorbent weight of 50.0 mg, and a contact time of 10 min. The adsorption isotherms of the contaminants on the nanocomposite were analyzed using the Freundlich model, indicating a heterogeneous distribution of active sites on the adsorbent surface. The highest adsorption capacity of MB and CR is 135.1 and 285.7 $mg.g^{-1}$, respectively. Moreover, Fe_3O_4/GO nanocomposite recycled five cycles with proper adsorption capacity. Overall, the Fe_3O_4/GO nanocomposite holds great promise for efficient and sustainable water treatment, providing safe and clean water globally.

INTRODUCTION

Water pollution is a significant environmental and health problem, with various sources of contamination, including industrial and domestic waste, agricultural practices, and natural disasters such as floods and landslides (Akhtar et al. 2021, Luo et al. 2022, Peters & Meybeck 2000). Dyes play a significant role as pollutants in wastewater, posing a considerable threat to human health due to their persistent and non-biodegradable properties. Dyes are categorized based on the charge of their chromophore group, namely cationic, anionic, and non-ionic dyes, the latter being insoluble in water (Maheshwari et al. 2021). Congo red (CR) is a well-known anionic diazo dye widely used in the textile industry, laboratory research, and staining applications. On the other hand, methylene blue (MB) is a basic dye applied widely by textile and paper industries to scientific research and medical practices. This versatile dye has exceptional color stability and water solubility (Heo et al. 2022, Lachheb et al. 2002). Both MB and CR dyes pose severe risks to human health, including gastrointestinal illnesses, skin diseases, and even cancer (Halim et al. 2015, Thattil & Leema Rose 2019). Therefore, developing efficient and sustainable water treatment technologies is essential for ensuring access to safe and clean water.

In recent years, nanotechnology has emerged as a promising water treatment approach due to nanoparticles' unique properties (Gehrke et al. 2015, Qu et al. 2013, Theron et al. 2008). Nanoparticles have a high surface-to-volume ratio, enhancing their reactivity and allowing for the development of more efficient and effective water treatment technologies (Cele 2020, Saikia et al. 2019, Vaghari et al. 2016).

The Fe_3O_4/graphene oxide (Fe_3O_4/GO) composite has received considerable attention among the various nanoparticles due to its excellent adsorption and photocatalytic properties (Ouyang et al. 2015, Yao et al. 2012). Fe_3O_4 nanoparticles possess magnetic properties, which enable easy separation of the nanocomposite from treated water using an external magnetic field. GO has a large specific surface area and high reactivity, making it an ideal support material for

Fe_3O_4 nanoparticles. Studies on the removal of CR and MB from aqueous solution based on Fe_3O_4/GO nanoparticles and their adsorption mechanism are still lacking.

In this study, Fe_3O_4/GO nanocomposite was synthesized and tested for its efficiency in removing two contaminants, namely methylene blue (MB) and congo red (CR), from water. Different experimental factors, such as pH, the weight of the adsorbent, and the contact time, were investigated to determine their impact on the adsorption efficiency of Fe_3O_4/GO nanocomposites. Additionally, the viability of recycling the material to maintain its adsorption capacity for MB and CR was evaluated.

MATERIALS AND METHODS

Materials and Chemicals

The materials used in this study include methylene blue ($C_{16}H_{18}ClN_3S$), congo red ($C_{32}H_{22}N_6Na_2O_6S_2$), iron(II) chloride tetrahydrate ($FeCl_2.4H_2O$), iron(III) chloride hexahydrate ($FeCl_3.6H_2O$), graphite, sodium hydroxide (NaOH), hydrochloric acid (HCl), sulfuric acid (H_2SO_4), hydrogen peroxide (H_2O_2), potassium permanganate ($KMnO_4$), and sodium nitrate ($NaNO_3$). All chemicals were purchased from Sigma-Aldrich (St. Louis, MO, USA) and Merck (Darmstadt, Germany). Deionized (DI) water was used in all experiments.

Instrumentation

The equipment used in this study includes a magnetic stirrer, pH meter, ultraviolet-visible (UV-Vis) spectrophotometer (Genesys 10s, USA), and centrifuge (Hettich Zentrifugen, Germany). The adsorptions of MB and CR were measured at 665 nm, 498 nm, and 510 nm, respectively. The morphology and structure of the Fe_3O_4/GO composite were characterized using scanning electron microscopy (SEM) (TM 4000 plus Hitachi) and X-ray diffraction (XRD) (MiniFlex 600 Rigaku) employing CuK_α (λ=1.5418 Å, 2Θ/steps = 0.03 °/step). Fourier transform infrared spectroscopy (FTIR) in the range 4000 to 400 cm^{-1} was carried out using FT/IR-4600 Jasco. The surface area was observed by Brunauer–Emmett–Teller (Micromeritics Tristar II 3020). Magnetic measurements were made using a vibrating sample magnetometer (VSM) at room temperature.

Synthesis of Fe_3O_4/GO Nanocomposite

To synthesize GO, natural graphite powder was subjected to a modified Hummer's method (Zaaba et al. 2017). In brief, 3 g graphite powder was added to 42 mL H_2SO_4 98% and cooled under vigorous stirring. $KMnO_4$ was added steadily and kept at a temperature of up to 35°C, vigorous stirring for 30 min. DI water was added slowly, and the mixture was kept under 50°C, stirring for 1 h. The mixture was washed with H_2O_2, HCl, and DI water and dried under vacuum at 50°C.

To synthesize Fe_3O_4/GO, 5,79 g of $FeCl_2.4H_2O$ and 8,1 g of $FeCl_3.6H_2O$ were dissolved in 200 mL of DI water and homogenized solution of dispersed graphene oxide with ultrasonic vibration. Afterward, a vigorous stirring process was employed to add NaOH until the pH reached approximately 12. Subsequently, the mixture was heated to 150°C in a Teflon-lined autoclave for 7 h. The resulting mixture was then separated by centrifugation, followed by multiple washes with ethanol and water. Finally, it was dried at 80°C for 12 h.

Procedure

Batch adsorption studies were conducted to evaluate the Fe_3O_4/GO nanocomposite's efficiency for removing MB and CR from samples. In each experiment, a known amount of the Fe_3O_4/GO nanocomposite was added to a 50 mL aqueous solution of the contaminant with an initial concentration of 10 to 500 $mg.L^{-1}$. The solution was ultrasonic vibration for 5 min and stirred for 30 min. After that, the solution was kept at room temperature. The Fe_3O_4/GO nanocomposite was separated from the solution by magnetic separation and centrifugation, and the residual concentration of the contaminant was measured using a UV-Vis spectrophotometer. The efficiency of adsorbate removal (*AR*) and adsorption capacity of equilibrium () was calculated using the following equation:

$$AR\ \% = \frac{C_0 - C_t}{C_0} x100$$

$$q_e = \frac{V(C_0 - C_t)}{m}$$

Where C_0 is the initial concentration, C_t is the MB or CR concentration at time t, respectively. m is the amount of used adsorbents, V is the solution volume.

RESULTS AND DISCUSSION

Characterization of Fe_3O_4/GO Nanocomposite

Fig. 1 displays the Fourier-transform infrared (FTIR) spectra of the adsorbent in the range of 400-4000 cm^{-1}. The peak at about 582 cm^{-1}, which indicates the vibration of the Fe-O bond, corresponds to the formation of Fe_3O_4 in the adsorbent (Cao et al. 2014, Nguyen et al. 2020). The peak at 1384 and 1052 cm^{-1} were assigned to the two stretching vibration bands related to the C–O bond attached to the hydroxyl and carboxyl groups, respectively. Additionally, stretching

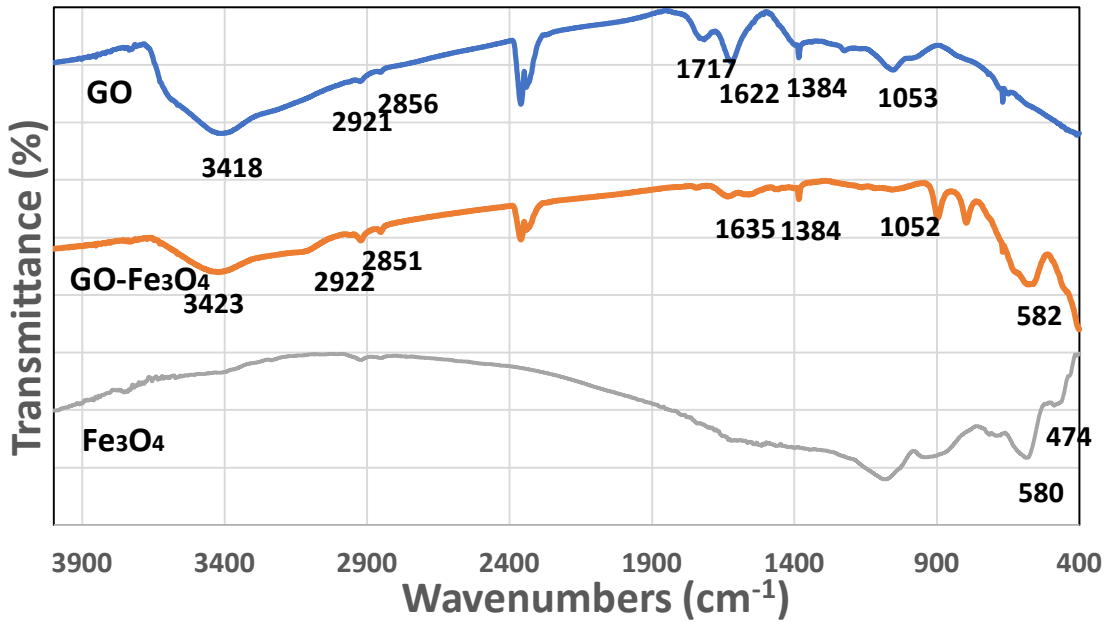

Fig. 1: FTIR spectra of the Fe_3O_4/GO nanocomposite.

vibrations of C=C are identified at 1635 cm^{-1}. The stretching vibration bands related to the C = O bond of the carboxyl group can be seen at 1717 cm^{-1}. The stretching vibration of the O-H bond was observed as a strong vibration in the range of around 3423 cm^{-1}. These findings aligned with previous studies (Cui et al. 2015, Liu et al. 2014, Ye et al. 2014). Consequently, these findings confirm the successful synthesis of the Fe_3O_4/GO adsorbent, in which all functional groups act as sites for adsorption and substantially contribute to capturing MB and CR from the samples.

The X-ray diffraction (XRD) patterns of the Fe_3O_4/GO are shown in Fig. 2. The peaks can be seen at $2\theta = 30.1^o$ (220), 35.5^o (311), 43.1^o (400), 53.1^o (422), 57.1^o (511), and 62.5^o (440). By comparing the angle pattern observed in the XRD analysis with the standard Fe_3O_4 compound card (JCPDS file no. 190629), it could be concluded that the composite being studied was consistent with the magnetite phase (He & Gao 2011). These findings provide crucial information on the crystallographic properties of Fe_3O_4/GO, which was essential in understanding the adsorption behavior of the nanocomposite.

Fig. 3 displays SEM images of Fe_3O_4/GO nanocomposite samples captured at different magnifications. The images reveal that spherical magnetic nanoparticles ranged in size from 30 to 100 nm and were located on the surface of GO. The adsorption-desorption isotherm is shown in Fig. 4. The specific surface area of Fe_3O_4/GO nanocomposite is 604.57

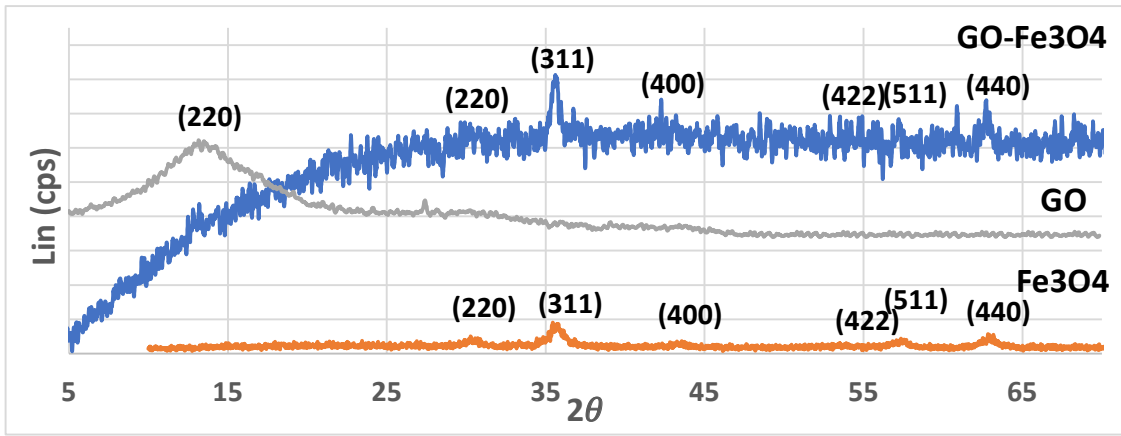

Fig. 2: XRD patterns of the Fe_3O_4/GO nanocomposite.

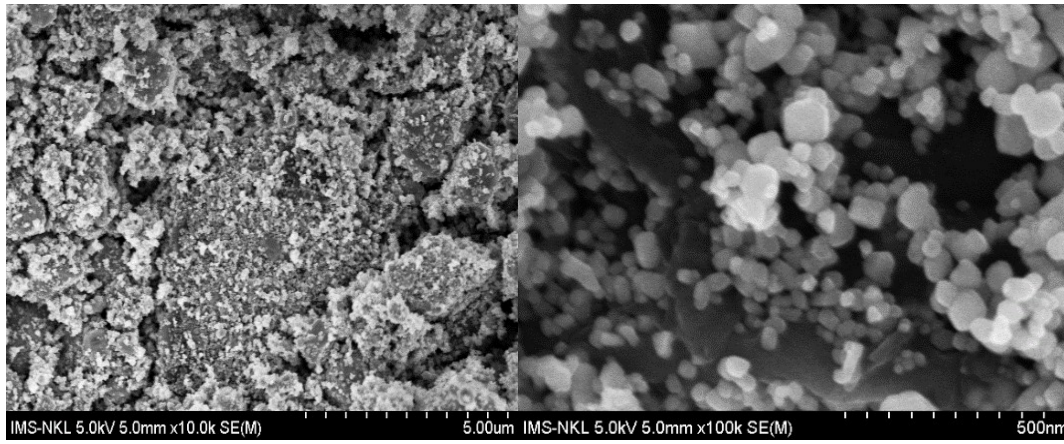

Fig. 3: SEM image of Fe_3O_4/GO nanocomposite.

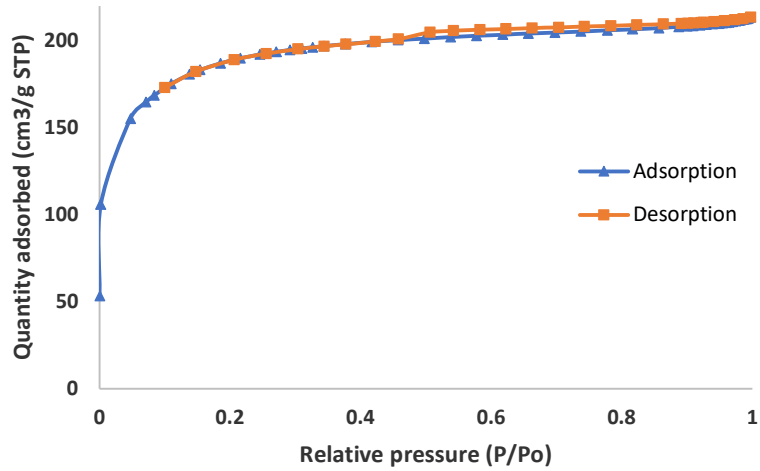

Fig. 4: N_2 adsorption and desorption isotherms of Fe_3O_4/GO nanocomposite.

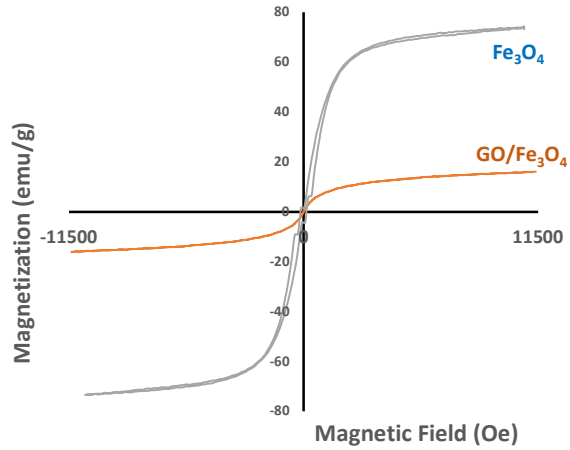

Fig. 5: Magnetic hysteresis loop of Fe_3O_4/GO nanocomposites and Fe_3O_4.

$m^2.g^{-1}$, which is higher than the reported values (Liu et al. 2012, Mahvi et al. 2021).

Fig. 5 presents the magnetization hysteresis curves of Fe_3O_4/GO, which were measured under room temperature conditions. The saturation magnetization of Fe_3O_4/GO was determined to be 15.91 $emu.g^{-1}$, demonstrating a lower value compared to that of Fe_3O_4 (73.55 $emu.g^{-1}$). This reduction in saturation magnetization can be attributed to the lower concentration of Fe_3O_4 within Fe_3O_4/GO, which was caused by the presence of the non-magnetic component GO. The graph in Fig. 5 reveals that the remanence magnetization and coercivity values of Fe_3O_4/GO were remarkably low, indicating that Fe_3O_4/GO exhibited superparamagnetic behavior at room temperature. The superparamagnetic properties of Fe_3O_4/GO suggest that it could be readily separated from water by applying a magnetic field. Furthermore, upon removal of the magnetic field, Fe_3O_4/GO can disperse effectively within a reaction solution.

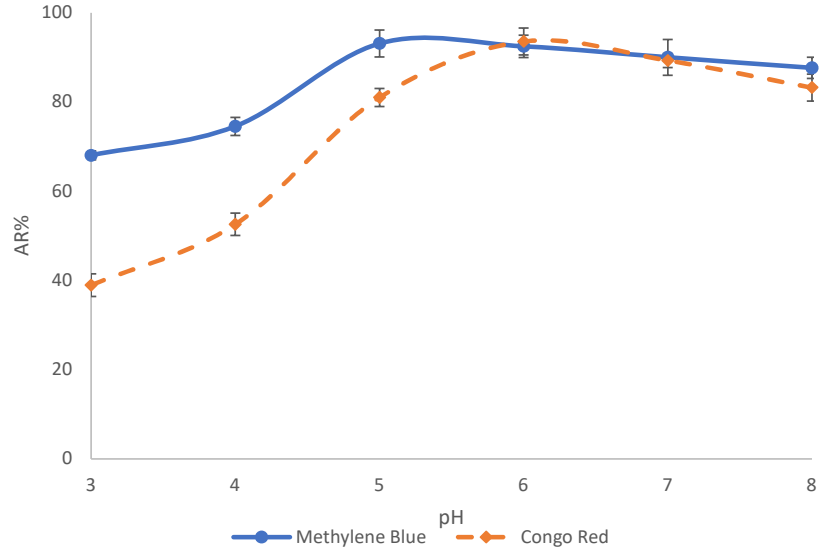

Fig. 6: Influence of pH on the removal of MB and CR.

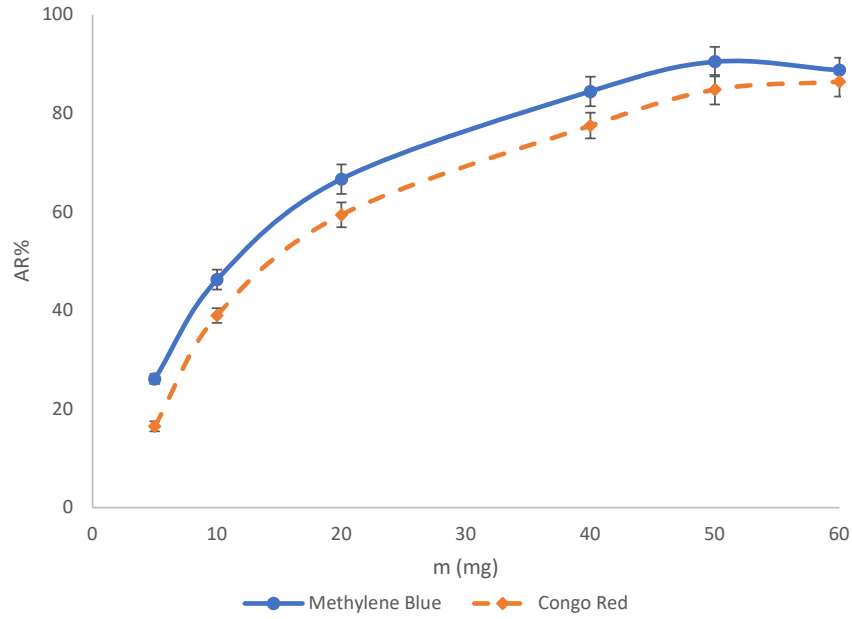

Fig. 7: Influence of the amount of adsorbent (m) on the removal of MB and CR.

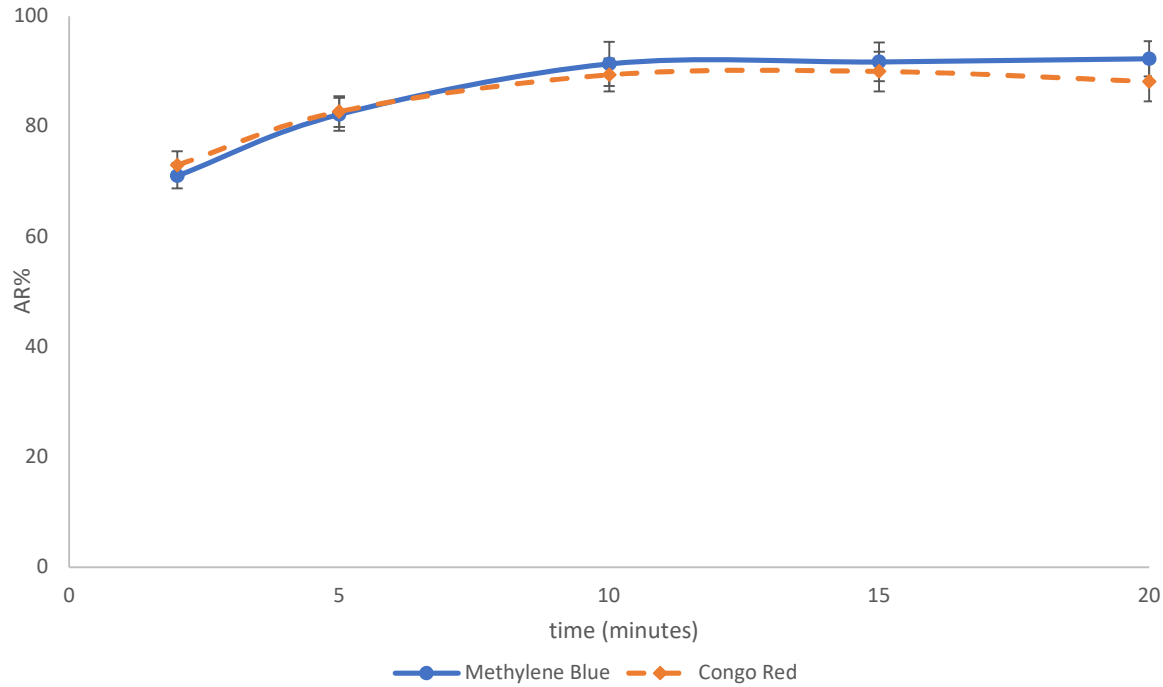

Fig. 8: Influence of the time (min) on the removal of MB and CR.

Factors Affecting the Adsorption Efficiency

The adsorption recovery of MB and CR was studied over a pH range of 3.0 to 8.0. Fig. 6 shows that the maximum adsorption was obtained at pH 6.0 for MB and CR. The pH_{pzc} value of Fe_3O_4/GO was 6.2 (Mahvi et al. 2021, You et al. 2019). At pH 6.0 below the pH_{pzc}, the surface of the adsorbent was positively charged. The pKa values of MB and CR are 3.8 and 4.5, respectively. Therefore, at a solution's pH above pKa, the MB and CR exist in anionic speciations. The recovery of MB and CR through adsorption could be attributed to the electrostatic attraction between the adsorbent's surface and the analytes. Comparable findings have been documented in existing literature (Cheng et al. 2019, Yousef & El-Eswed 2009, Yu et al. 2016). Therefore, a pH of 6.0 was used for MB and CR as the optimal pH value.

The adsorption recovery can be influenced by the amount of adsorbent used. The quantities of the adsorbent (ranging from 5.0 to 60.0 mg) affected the retrieval of MB and CR was examined. This was accomplished by introducing varying amounts of the nanocomposite into the sample solutions. As depicted in Fig. 7, an increase in the amount of adsorbent resulted in a higher recovery due to the availability of additional adsorption sites. However, once the extraction of the analytes reached saturation, further increases in the adsorbent amount did not lead to a proportional increase in extraction, resulting in wastage. The best results were obtained when 50.0 mg of the adsorbent was utilized in the following experiments.

In addition to the adsorbent amount, the contact time (ranging from 2.0 to 20.0 min) played a significant role in the adsorption process of the Fe_3O_4/GO nanocomposite. Fig. 8 illustrates the effect of time on the removal of MB and CR. The results demonstrate that initially, the adsorption of both dyes increased with longer times due to the availability of more active adsorption sites. However, the recovery eventually reached a constant value as the number of accessible active adsorption sites decreased. Therefore, a contact time of 10.0 min was chosen for subsequent experiments.

Furthermore, it was carefully selected a desorbing agent that fulfilled specific criteria: it had to be cost-effective, environmentally friendly, effective in desorption, and not cause any damage to the structure of the adsorbent. Fe_3O_4/GO nanocomposite used is dispersed in weak acidic environments, 20 mL of distilled water and acetic acid, ultrasound vibration for 5 min, then washed with magnets. This process is repeated 2 times. Next, wash the material with distilled water twice at 40°C, then wash with ethanol at 40°C. Finally, the material is dried at 60°C overnight. The ability of the adsorbent to be reused was assessed, and Fig. 9 illustrates that even after undergoing five cycles, the adsorbent maintained effective adsorption recovery, demonstrating its suitability for repeated utilization.

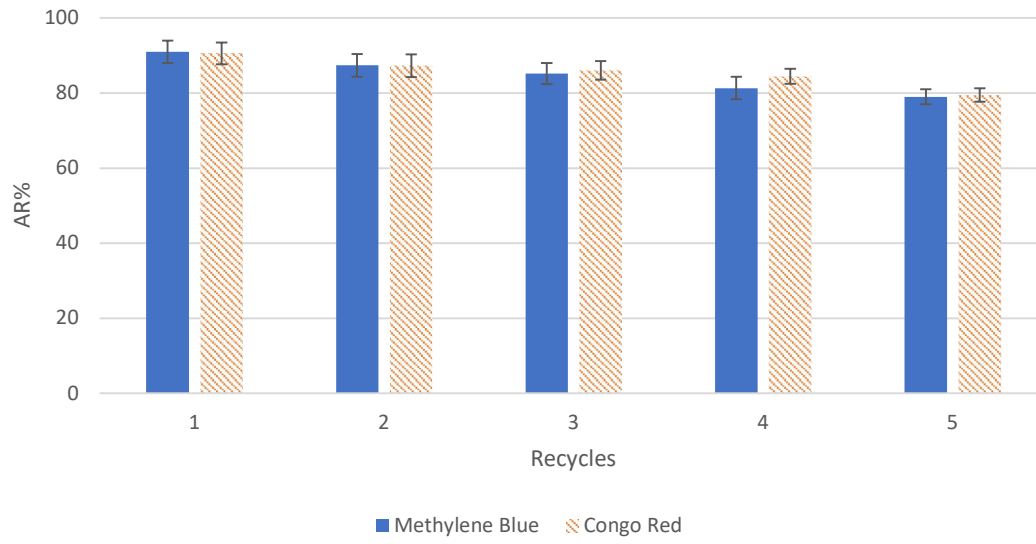

Fig. 9: Reusability study of Fe_3O_4/GO nanocomposite (pH = 6.0, time 10 min and amount of adsorbent 50.0 mg).

The adsorption process is driven by the affinity between the adsorbate and the surface of the adsorbent, and it continues until the system reaches dynamic equilibrium. Adsorption isotherms can describe the relationship between the adsorbate and the adsorbent surface. The Langmuir model (1) is suitable for analyzing monolayer adsorption, while the Freundlich model (2) applies to heterogeneous surfaces and multilayer adsorption.

$$\frac{C_e}{q_e} = \frac{1}{q_m K_L} + \frac{C_e}{q_m} \quad ...(1)$$

$$\ln q_e = \ln K_F + (1/n) \ln C_e \quad ...(2)$$

Where C_e is the equilibrium concentration ($mg.L^{-1}$); q_e is the amount of adsorbed analyte per unit mass of the adsorbent, and q_m is the maximum adsorption capacity ($mg.g^{-1}$); K_L is the Langmuir constant ($L.mg^{-1}$) related to the energy of adsorption; is the adsorption intensity; K_F and $1/n$ Are Freundlich constants related to adsorption capacity and intensity of adsorption, respectively.

Table 1: Parameters and the correlation coefficients fitted by Langmuir and Freundlich models of MB and CR onto Fe_3O_4/GO nanocomposite.

		Methylene Blue	Congo Red
Langmuir model	q_m [$mg.g^{-1}$]	135.1	285.7
	K_L [$L.mg^{-1}$]	0.0316	0.0071
	R^2	0.9075	0.9246
Freundlich model	K_F [$mg.g^{-1}$]	1.531	0.486
	N	1.31	0.96
	R^2	0.9897	0.9877

Table 1 presents the key parameters, including n, K_F, K_L, and q_m, along with the determination coefficient (R^2) of the adsorption models. The outcomes suggest that the experimental data aligns well with the Freundlich model within the investigated range, as indicated by its higher R^2 value compared to the Langmuir model for three analytes. This observation could be attributed to the uneven distribution of active sites on the surface of the adsorbent. The favorable isotherm of the Freundlich model may be

Table 2: Comparison of maximum adsorption capacity of Fe_3O_4/GO and other adsorbents.

Adsorbents	Maximum adsorption capacity (mg/g)		References
	MB	CR	
Wheat shells (WHS)	16.56	-	(Bulut & Aydın 2006)
Halloysite nanotubes (HNTs)	84.32	-	(Zhao & Liu 2008)
Graphene	153.85	-	(Liu et al. 2012)
Activated biochar (CO_2–biochar)	161	-	(Franciski et al. 2018)
Zn-Fe_2O_4 nanospheres	-	16.58	(Rahimi et al. 2011)
Maghemite nanoparticles (γ-Fe2O3)	-	208.33	(Afkhami & Moosavi 2010)
Anilinepropylsilica xerogel (SiAn)	-	22.62	(Pavan et al. 2008)
Unmodified fly ash	-	22.12	(Harja et al. 2022)
Fe_3O_4/GO	135.1	285.7	This work

attributed to the low oxidation degree(Yan et al. 2014). According to Langmuir isotherm, the maximum monolayer adsorption capacity of MB and CR at equilibrium is 135.1 and 285.7 $mg.g^{-1}$, respectively.

Table 2 compares the ability to adsorb MB and CR using Fe_3O_4/GO and other adsorbents. The findings indicate that Fe_3O_4/GO performed exceptionally well as an adsorbent, showing a comparatively higher adsorption capacity for MB and CR than the other materials tested.

CONCLUSIONS

Overall, the results of this study indicate that the Fe_3O_4/GO nanocomposite is an effective adsorbent for removing MB and CR from water. A composite material, Fe_3O_4/GO, was synthesized and employed to capture MB and CR from a sample. The adsorbent proved to be highly effective for both MB and CR. By optimizing the conditions, the pH level of 6.0, an adsorbent quantity of 50.0 mg, and an adsorption time of 10.0 min were identified as the ideal values. Equilibrium data for the adsorption of both substances were gathered using the Langmuir and Freundlich models, two different isotherm models. The determination coefficient of the Freundlich model surpassed that of the Langmuir model. The maximum capacity for monolayer adsorption was 135.1 $mg.g^{-1}$ for MB and 285.7 $mg.g^{-1}$ for CR. These results indicated that the proposed adsorbent possessed exceptional adsorption capabilities. Moreover, the adsorbent could be reused up to five times without declining performance, leading to cost savings.

ACKNOWLEDGMENTS

This work was supported by Hung Vuong University through the project "Synthesis of Fe_3O_4/graphene oxide nanocomposite for the treatment of organic contaminants". We would like to thank the peer reviewers for their valuable suggestions and comments that improved this paper.

REFERENCES

Afkhami, A. and Moosavi, R. 2010. Adsorptive removal of Congo red, a carcinogenic textile dye, from aqueous solutions by maghemite nanoparticles. J. Hazard. Mater., 174(1-3): 398-403.

Akhtar, N., Syakir Ishak, M.I., Bhawani, S.A. and Umar, K. 2021. Various natural and anthropogenic factors responsible for water quality degradation: A review. Water, 13(19): 456

Bulut, Y. and Aydın, H. 2006. A kinetics and thermodynamics study of methylene blue adsorption on wheat shells. Desalination, 194(1): 259-267.

Cao, C., Xiao, L., Chen, C., Shi, X., Cao, Q. and Gao, L. 2014. In situ preparation of magnetic Fe3O4/chitosan nanoparticles via a novel reduction-precipitation method and their application in adsorption of reactive azo dye. Powder Technol., 260: 90-97.

Cele, T. 2020. Preparation of nanoparticles. Eng. Nanomater. Saf., 5: 11-21.

Cheng, J., Sun, Z., Yu, Y., Li, X. and Li, T. 2019. Effects of modified carbon black nanoparticles on plant-microbe remediation of petroleum and heavy metal co-contaminated soils. Int. J. Phytoremed., 21(7): 634-642.

Cui, L., Wang, Y., Gao, L., Hu, L., Yan, L. and Wang, Y. 2015. EDTA functionalized magnetic graphene oxide for removal of Pb(II), Hg(II), and Cu(II) in water treatment: Adsorption mechanism and separation property. Chem. Eng. J., 281: 1-10.

Franciski, M.A., Peres, E.C., Godinho, M., Perondi, D., Foletto, E.L. and Oliveira, M.L.S. 2018. Development of CO2-activated biochar from solid wastes of a beer industry and its application for methylene blue adsorption. Waste Manag., 78: 630-638.

Gehrke, I., Geiser, A. and Somborn-Schulz, A. 2015. Innovations in nanotechnology for water treatment. Nanotechnol. Sci. Appl., 8: 1-17.

Halim, A.A., Han, K.K. and Hanafiah, M.M. 2015. Removal of methylene blue from dye wastewater using river sand by adsorption. Nat. Environ. Pollut. Technol., 14(1): 89-94.

Harja, M., Buema, G. and Bucur, D. 2022. Recent advances in the removal of Congo Red dye by adsorption using industrial waste. Sci. Rep., 12(1):1-18.

He, H. and Gao, C. 2011. Synthesis of Fe3O4/Pt nanoparticles decorated carbon nanotubes and their use as magnetically recyclable catalysts. J. Nanomater, 19: 35.

Heo, J.W., An, L., Chen, J., Bae, J.H. and Kim, Y.S. 2022. Preparation of amine-functionalized lignins for the selective adsorption of Methylene blue and Congo red. Chemosphere, 295: 313.

Lachheb, H., Puzenat, E., Houas, A., Ksibi, M., Elaloui, E. and Guillard, C. 2002. Photocatalytic degradation of various types of dyes (Alizarin S, Crocein Orange G, Methyl Red, Congo Red, Methylene Blue) in water by UV-irradiated titania. Appl. Catal. B Environ., 39(1): 75-90.

Liu, L., Zhang, Y., He, Y., Xie, Y., Huang, L. and Wang, Y. 2014. Preparation of montmorillonite-pillared graphene oxide with increased single- and co-adsorption towards lead ions and methylene blue. RSC Adv., 5(6): 3965-3973.

Liu, T., Li, Y., Du, Q., Sun, J., Jiao, Y. and Liu, Y. 2012. Adsorption of methylene blue from aqueous solution by graphene. Coll. Surf. B Biointerf., 90(1): 197-203.

Luo, P., Mu, Y., Wang, S., Zhu, W. and Mishra, B.K. 2022. Exploring sustainable solutions for the water environment in Chinese and Southeast Asian cities. Ambio., 51(5): 1199-1218.

Maheshwari, K., Agrawal, M. and Gupta, A.B. 2021. Dye Pollution in Water and Wastewater. In: Muthu, S.S. and Khadir, A. (eds), Novel Materials for Dye-Containing Wastewater Treatment, Springer, Singapore, pp. 1-25.

Mahvi, A.H., Balarak, D. and Bazrafshan, E. 2021. Remarkable reusability of magnetic Fe_3O_4-graphene oxide composite: A highly effective adsorbent for Cr(VI) ions. Int. J. Environ. Anal. Chem., 5: 1-21.

Nguyen, V.H., Van, H.T., Nguyen, V.Q., Dam, X. and Hoang, L.P. 2020. Magnetic Fe_3O_4 nanoparticle biochar derived from Pomelo peel for reactive red 21 adsorption from aqueous solution. J. Chem., 2: 1-11.

Ouyang, K., Zhu, C., Zhao, Y., Wang, L., Xie, S. and Wang, Q. 2015. Adsorption mechanism of magnetically separable Fe3O4/graphene oxide hybrids. Appl. Surf. Sci., 355: 562-569.

Pavan, F.A., Dias, S.L.P., Lima, E.C. and Benvenutti, E.V. 2008. Removal of Congo red from aqueous solution by anilinepropylsilica xerogel. Dye Pigm., 76(1): 64-69.

Peters, N.E. and Meybeck, M. 2000. Water quality degradation effects on freshwater availability: Impacts of human activities. Water Int., 25(2): 185-193.

Qu, X., Alvarez, P.J.J. and Li, Q. 2013. Applications of nanotechnology in water and wastewater treatment. Water Res., 47(12): 3931-3946.

Rahimi, R., Kerdari, H., Rabbani, M. and Shafiee, M. 2011. Synthesis, characterization and adsorbing properties of hollow Zn-Fe_2O_4 nanospheres on removal of Congo red from aqueous solution. Desalination, 280(1-3): 412-418.

Saikia, J., Gogoi, A. and Baruah, S. 2019. Nanotechnology for water remediation. In: Dasgupta, N., Ranjan, S. and Lichtfouse, E. (eds), Environmental Nanotechnology, Volume 2, Springer, Cham, pp. 195-211.

Thattil, P.P. and Leema Rose, A. 2019. Photodegradation of Congo red dye via simple and effective air oxidation using copper(II) chloride and sunlight. Nat. Environ. Pollut. Technol., 18(4): 1243-1248.

Theron, J., Walker, J.A. and Cloete, T.E. 2008. Nanotechnology and water treatment: Applications and emerging opportunities. Crit. Rev. Microbiol., 34(1): 43-69.

Vaghari, H., Jafarizadeh-Malmiri, H., Mohammadlou, M., Berenjian, A. and Anarjan, N. 2016. Application of magnetic nanoparticles in smart enzyme immobilization. Biotechnol. Lett., 38(2): 223-233.

Yan, H., Tao, X., Yang, Z., Li, K. and Yang, H. 2014. Effects of the oxidation degree of graphene oxide on the adsorption of methylene blue. J. Hazard. Mater., 268: 191-198.

Yao, Y., Miao, S., Liu, S., Ma, L.P., Sun, H. and Wang, S. 2012. Synthesis, characterization, and adsorption properties of magnetic Fe_3O_4@ graphene nanocomposite. Chem. Eng. J., 184: 326-332.

Ye, N., Xie, Y., Shi, P., Gao, T. and Ma, J. 2014. Synthesis of magnetite/ graphene oxide/chitosan composite and its application for protein adsorption. Mater. Sci. Eng., 45: 8-14.

You, N., Wang, X.F., Li, J.Y., Fan, H.T., Shen, H. and Zhang, Q. 2019. Synergistic removal of arsanilic acid using adsorption and magnetic separation technique based on Fe_3O_4@graphene nanocomposite. J. Ind. Eng. Chem., 70: 346-354.

Yousef, R.I. and El-Eswed, B. 2009. The effect of pH on the adsorption of phenol and chlorophenols onto natural zeolite. Coll. Surf. A Physicochem. Eng. Asp., 334(1-3): 92-99.

Yu, L., Chen, J., Liang, Z., Xu, W., Chen, L. and Ye, D. 2016. Degradation of phenol using Fe_3O_4-GO nanocomposite as a heterogeneous photo-Fenton catalyst. Sep. Purif. Technol., 171: 80-87.

Zaaba, N.I., Foo, K.L., Hashim, U., Tan, S.J., Liu, W.W. and Voon, C.H. 2017. Synthesis of graphene oxide using modified hummers method: Solvent influence. Procedia Eng., 184: 469-477.

Zhao, M. and Liu, P. 2008. Adsorption behavior of methylene blue on halloysite nanotubes. Micropor. Mesopor. Mater., 112(1-3): 419-424.